A review on mitigation technologies of low frequency current ripple injected into fuel cell and a case study

Yuedong Zhan [a, *], Youguang Guo [b], Jianguo Zhu [c], Bo Liang [d], Biao Yang [a]

[a] Department of Automation, Kunming University of Science and Technology

Kunming, 650500, China

[b] School of Electrical and Data Engineering, University of Technology Sydney

Sydney, NSW 2007, Australia

[c] School of Electrical & Information Engineering, The University of Sydney

Sydney, NSW 2006, Australia

[d] School of Materials and Energy, Guangdong University of Technology,

Guangzhou, 510006, China

(Emails: ydzhan@163.com, youguang.guo-1@uts.edu.au, jianguo.zhu@sydney.edu.au,

liangbo@gdut.edu.cn, yb_chenggong@163.com)

*Corresponding author: Tel.: +86 871 65916596; Fax: +86 871 65916596,

Email address: ydzhan@163.com (Yuedong Zhan)

ABSTRACT

In this paper, the state-of-the-art of mitigation technologies of low frequency current ripple (LFCR) injected into fuel cell (FC) are reviewed. Although there are their own merits and demerits, the optimized LFCR control techniques and topology structures are characterized in many aspects like performance, durability, reliability and lifetime of FC. Three mains topologies and mitigation methods of LFCR have been

investigated based on the literature review, which are the passive compensation approaches, active compensation approaches, and passive and active hybrid compensation methods. Some rules based tables are set to evaluate the LFCR against the topologies, control strategies, current ripple, application and advantages/limitations. Moreover, the mitigation control strategies are compared side by side with their specific applications in FC system. To select and implement them, this review can provide a reference and basis for the researchers in related fields. Finally, a case study in an uninterruptible power supply (UPS) application is conducted.

Nomenclature	
AC	Alternative current
CBP	Cascaded boost and push-pull converter
CCM	Continuous conduction mode
CFBC	Current-fed boost converter
CFDHB	Current-fed dual half-bridge
DAB	Dual active bridge
DBI	Differential boost inversion
DC	Direct current
DCM	Discontinuous conduction mode
DICM	Discontinuous inductor conduction mode
DSP	Digital signal processor
EPLD	Electrically programmable logic device
EV	Electric vehicle
FC	Fuel cell
FCEV	Fuel cell electric vehicle
FIBC	Floating interleaved boost converter
FPGA	Field-programmable gate array
IBC	Interleaved boost converter

LFCR	Low frequency current ripple
LFSC	Line frequency switched cycloconverter
MPPT	Maximum power point tracking
NNC	Neural network control
NSS	Natural switching surface
OCV	Open circuit voltage
PCS	Power conditioning system
PEMFC	Proton exchange membrane fuel cell
PFC	Power factor correction
PGS	Power generation system
PI	Proportional integral control
PLL	Phase-locked-loop
PP	Push-pull DC/DC converter
PR	Proportional resonant control
PSFB	Parallel/series full-bridge
PSP	Phase shifted boost and push-pull converter
SC	Supercapacitor
SCC	Series connected converters
SMC	Sliding mode control
SOFC	Solid oxide fuel cell
STP	Standard temperature and pressure
UPS	Uninterruptible power supply
ZVS	Zero-voltage switching

1

2 1. Introduction

3   Proton exchange membrane fuel cell (PEMFC) is much suitable for a continuous

4 power source, which has high power density, long reliable run-time, and low operating

5 temperature as a fuel cell (FC) power generation system (PGS). However, because of

6 generating an low DC voltage, the PEMFC must employ a power conditioning system

7 (PCS), such as a DC/DC converter to promote the low DC voltage to a higher one, or a

8 DC/AC inverter to acquire an AC voltage. Meanwhile, there are severe current ripples,

9 including the low frequency current ripples (LFCR) and harmonics in the side of DC

10   bus.

In practical FC PGS applications, Gemmen [1] provided a first attempt to examine the influence of inverter load current ripple on FC operation condition in 2003. The LFCR was found to be the major reason of performance degradation and lifetime reduction of PEMFC when the loads change in a solid oxide fuel cell (SOFC) [2] and a PEMFC stack [3]. Moreover, Wahdame *et al.* [4] investigated the impact of the DC/DC power converter current ripples on the durability of PEMFC stack.

Because a power converter and its control strategy play a significant role on the reliability and durability of FC PCS, many scholars have recently studied novel DC/DC and DC/AC power converter topologies and some mitigation methods of LFCR and low-current ripples in FC PCS [5-12]. Recently, some papers related to DC/DC converters reducing the current ripple in the low-voltage DC side have been figured out in literature. Moreover, this field has become a research direction and hotspot. A 6-phase interleaved boost converter (IBC) with semiconductors and inverse coupled inductors for PEMFC vehicles has been proposed, which has the advantages of low-current ripple, high voltage conversion ratio, high efficiency, high compactness and high redundancy [13]. A bidirectional DC/DC converter with coupled inductor for FC vehicles [14] and a quadratic buck-boost converter [15] was employed, which can achieve a tiny input and output current ripple and wide voltage conversion range. An interleaved boost converter topology with a multilevel diode clamped inverter was proposed, which has achieved obtaining the high voltage gain ratio, mitigating the input current ripple, and balancing the voltage across output capacitors [16]. An improved

floating interleaved boost converter (FIBC) with a small capacitor and a small inductor was proposed for FC applications, which can achieve zero input current ripple, high voltage gain, and low voltage stress [17]. A two-stage DC/DC/AC front-end boost converter with a new adaptive sliding mode control to reduce the influence of LFCR without impacting the dynamic performance was proposed, which can reduce the input current ripple, because the control function can cause the output impedance variation of the proposed boost converter [18].

Based on our research findings in this field, to control and restrict the LFCR within the required range, i.e. 5%, and extend the lifespan of FCs, three main kinds of LFCR topologies and mitigation methods have been studied and reviewed in the FC PCS, which are the passive compensation approaches, active compensation approaches, and passive and active hybrid compensation methods.

In this paper, Section 2 first details the generating mechanism of LFCR and the PEMFC stack equivalent circuit model. Secondly, the basic construction of FC PCS and performance effect of LFCR on PEMFC are introduced in Section 3. Then, for discussing the structure types, electrical characteristics, and application situations of power converters controlling the LFCR, a comprehensive review is followed with three main types of LFCR reduction strategies in Section 4, to assist the readers to master the recent topologies and their mitigation control strategies in FC PCS. Finally, a case study for a passive and active hybrid compensation method is conducted in Section 5. Moreover, the research trends in this field are proposed in the conclusion section.

1   ## 2. Generation mechanism and analysis of LFCR

2   To research the generation mechanism and spreading process of LFCR during

3   changing loads, a push-pull DC/DC converter and a single-phase half-bridge DC/AC

4   inverter system is employed as a case study, as depicted in Fig. 1, where I_{FC} and V_{FC}

5   are the voltage and current of PEMFC, I_{Bus} and V_{Bus} are the current and voltage of

6   DC bus, and i_o and v_o are the current and voltage of inverter output, respectively.

7

8
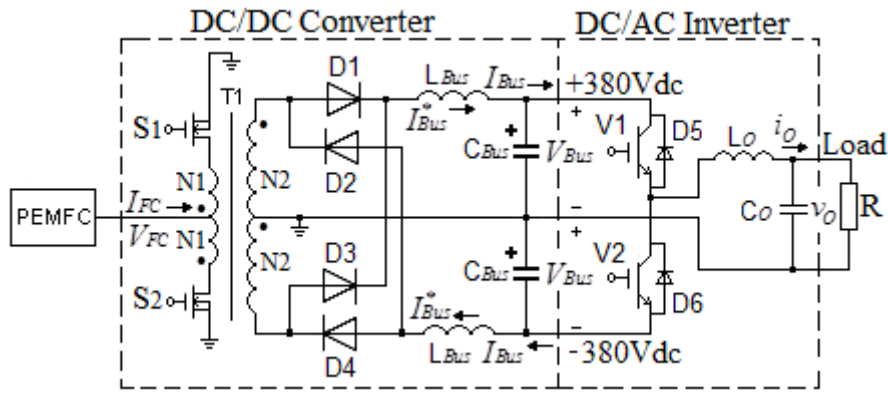
9   **Fig. 1** — Circuit structure of two-stage DC/DC converter and DC/AC inverter.

10

11   ## 2.1. Equivalent circuit model of PEMFC stack

12

13   According to the electrochemical energy conversion principle of PEMFC, the

14   output voltage of the stack is [19]:

15
$$V_{stack} = N \left\{ E^0 + \frac{RT}{2F} \ln \left[\frac{P_{H_2}(P_{O_2})^{\frac{1}{2}}}{P_{H_2O}} \right] + \frac{\Delta \bar{s}_{298.15K}}{nF}(T - 298.15) \right\}$$
$$- N \left\{ \frac{RT}{\alpha nF} \ln \left(\frac{i + i_n}{i_0} \right) + R_{Ohm}(i + i_n) + \frac{RT}{nF} \left(1 + \frac{1}{\alpha} \right) \ln \left[\frac{i_L}{i_L - (i + i_n)} \right] \right\}$$
(1)

16   where N is the number of cells of a PEMFC stack, n the number of electrons per

17   molecule of H_2 (2 electrons per molecule), α the transfer coefficient, T the operating

18   temperature of stack (K), R the universal gas constant (J/(mol·K)), F the Faraday's

19   constant (C/mol), R_{Ohm} the area-normalized Ohmic resistance of PEMFC ($\Omega \cdot cm^2$), i

the current density of stack (A/cm^2), i_L the limiting current density (A/cm^2), i_0 the

exchange current density (A/cm^2), i_n the internal current density (A/cm^2), P_i the partial

pressure of species i (i is H$_2$, O$_2$ or air, and the liquid water at cathode side) (kPa),

E^0 the single cell open circuit voltage (OCV) at the standard temperature and pressure

(STP), $E^0 = 1.23V$, and $\Delta \bar{s}_{298.15K}$ the molar entropy at STP (J/(mol·K)).

Based on the voltage output equation above and electrochemical reaction principle,

an equivalent circuit model of PEMFC are acquired, as depicted in Fig. 2 [20], where

R_{fc} and R_{fa} are the cathode and anode Faradaic resistances (Ω·cm^2), respectively,

reflecting the kinetics of the electrochemical reaction; C_{dlc} and C_{dla} are the cathode

and anode double-layer capacitances (F), respectively, indicating the double electrode

layer feature of the electrochemical reaction interface; and Z_W is the porous bounded

Warburg impedance, reflecting the mass transport model in FCs, which is expressed as

[19]:

$$Z_W = \frac{RT}{\sqrt{2\omega} A (n_i F)^2} \left(\frac{1}{c_i^0 \sqrt{D_i}} \right) (1-j) \tanh \left(\delta \sqrt{\frac{j\omega}{D_i}} \right) \qquad (2)$$

where A is the cathode electrode area (m^2), c_i^0 the cathode bulk concentration of

species i (mol/m^3), n_i the number of electrons per molecule of species i, δ the

thickness of diffusion layer (m), and D_i the diffusion coefficient of the species i

(m^2/s).
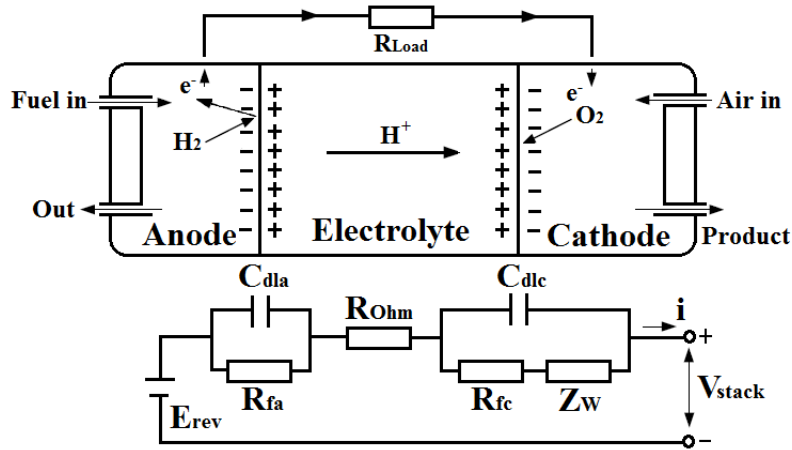
Fig. 2 — Equivalent circuit model diagram in a PEMFC [20].

2.2. Generation mechanism of LFCR

For the DC/AC inverter outputting a 50 Hz or 60 Hz sinusoidal waveform, its output current and voltage after filtering are determined by the expression:

$$i_o(t) = \sqrt{2} I_o \cos(\omega t + \varphi) \tag{3}$$

$$v_o(t) = \sqrt{2} V_o \cos(\omega t) \tag{4}$$

where I_o the output current for the inverter (A), V_o is the output voltage of the inverter (V), ω the angular frequency (rad/s), and φ the phase angle between the current and voltage (°).

Assume that there are no power losses in the UPS system. As the output voltage of PEMFC could be considered as current control voltage source, the input current of an FC is expressed as:

$$I_{FC}(t) = v_{Bus}(t) I_{Bus}^*(t) / V_{FC} \tag{5}$$

where

$$v_{Bus}(t) = V_{Bus} + \frac{1}{C_{Bus}} \int I_{Bus}^*(t) dt = V_{Bus} \left[1 + \frac{V_0 I_0}{2\omega C_{Bus} V_{Bus}^2} \sin(2\omega t + \varphi) \right] \tag{6}$$

1     $I_{Bus}^*(t) = \dfrac{P_o(t)}{V_{Bus}} = \dfrac{V_o I_o}{V_{Bus}} \left[\cos\varphi + \cos(2\omega t + \varphi) \right]$ (7)

2     $P_o(t) = V_{FC} I_{FC}(t) = V_{Bus} I_{Bus}^*(t) = v_o(t) i_o(t) = V_o I_o \left[\cos(2\omega t + \varphi) + \cos\varphi \right]$ (8)

3   where V_{Bus} is the DC bus filtered voltage (V), and I_{Bus}^* the DC bus filtered current (A),

4   which comprises a pure DC value and a 100 Hz or 120 Hz AC value. The I_{Bus} is the

5   input current of inverter (A), which is composed of I_{Bus}^* and the higher frequency

6   values ΔI_{Bus} because of the inverter switching mode of action.

7   Consequently, the LFCR injected into the FC stack could bring about adverse

8   effect on the voltage and current of FC, such as producing more heat, increasing the fuel

9   consumption, reducing the output power and efficiency of FC, and impacting its

10   availability [21].

11   As previously mentioned, when a PEMFC stack is with the LFCR , its output

12   current is:

13

14     $i = I_{DC} + I_{BUS} \sin(2\omega t + \theta)$ (9)

15

16   where I_{DC} is the DC side current value of the DC/DC converter load (A), I_{BUS}, ω, and

17   θ are the amplitude (A), angular frequency (rad/s) and phase (°) of the perturbation

18   signal from DC/DC converter, respectively.

19   When a PEMFC is without LFCR, based on the equivalent circuit model, as

20   depicted in Fig. 2, the total AC impedance is expressed as:

21

22     $Z(j\omega) = R_{Ohm} + \dfrac{R_{fa} \cdot \dfrac{1}{j\omega C_{dla}}}{R_{fa} + \dfrac{1}{j\omega C_{dla}}} + \dfrac{(R_{fc} + Z_W) \cdot \dfrac{1}{j\omega C_{dlc}}}{R_{fc} + Z_W + \dfrac{1}{j\omega C_{dlc}}}$ (10)

23

1   When a PEMFC is injected by LFCR, $Z_W\big|_{\omega\to 0} = R_{conc} = \delta\sigma_i\sqrt{\dfrac{2}{D_i}}$, where R_{conc} is

2 called as the concentration resistance indicating the mass transfer value in PEMFC, Eq.

3 (10) becomes:

$$Z'(j\omega) = R_{Ohm} + \frac{R_{fa}\cdot\dfrac{1}{j\omega C_{dla}}}{R_{fa}+\dfrac{1}{j\omega C_{dla}}} + \frac{(R_{fc}+R_{conc})\cdot\dfrac{1}{j\omega C_{dlc}}}{R_{fc}+R_{conc}+\dfrac{1}{j\omega C_{dlc}}}$$

4
$$= R_{Ohm} + \frac{R_{fa}}{1+\omega^2\tau_a^2} + \frac{R_{fc}+R_{conc}}{1+\omega^2\tau_c^2} - j\left[\frac{\omega\tau_a\cdot R_{fa}}{1+\omega^2\tau_a^2} + \frac{\omega\tau_c(R_{fc}+R_{conc})}{1+\omega^2\tau_c^2}\right]$$ (11)
$$= A(\omega)\angle\phi(\omega)$$

5 where $\tau_a = C_{dla}R_{fa}$ is the anode time constant (s), $\tau_c = C_{dlc}(R_{fc}+R_{conv})$ is the cathode

6 time constant (s), and $A(\omega)$ and $\phi(\omega)$ are the amplitude and phase shift (°) of

7 $Z(j\omega)$, respectively.

8   Fig. 4(c) shows the measured AC impedance variation of a 300 W air-breathing

9 and self-humidified, 63-cell PEMFC, when the frequency changes from 0 to 200 Hz

10 under the rated loads. Moreover, the lower the current ripple frequency, the higher the

11 PEMFC impedance. Hence, the current ripples including LFCR and harmonics will lead

12 to detrimental influences on the performance of PEMFC. Moreover, the LFCR has a

13 greater impact on FC performance, compared with the high-frequency current ripple.

14

15 **3. Basic construction of FC PCS and performance effect of LFCR on FC**

16   As shown in Fig. 3, there are two types of topological structure in an FC PCS. One

17 is the multiple-stage power converters, such as the two-stage DC/DC converters and

18 DC/AC inverters, and the other is the single-stage power converters, such as a

19 differential boost inversion (DBI). Moreover, the former has higher boost ratio and
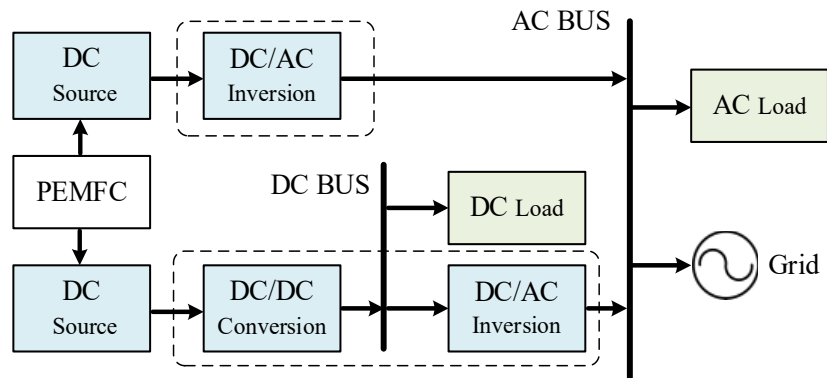
20 efficiency than the latter [22].

1
2   **Fig. 3** — Fundamental configuration for FC PCS.

3   The LFCR injected into a PEMFC will influence its performances, as depicted in

4   Fig. 4(a). Fig. 4(a) indicates that the voltage current waveform is a hysteresis

5   performance by simulating and testing the model parameters of a 300 W of PEMFC on

6   two different branches with LFCR and without LFCR. In the figure, the slope of the

7   major performance curve with LFCR is different from that of the reversal branch

8   without LFCR, which illustrates the performance degeneration of PEMFC with LFCR.

9   On the other hand, the current ripples could even shorten the lifetime of PEMFC, as

10   depicted in Fig. 4(b) [23].
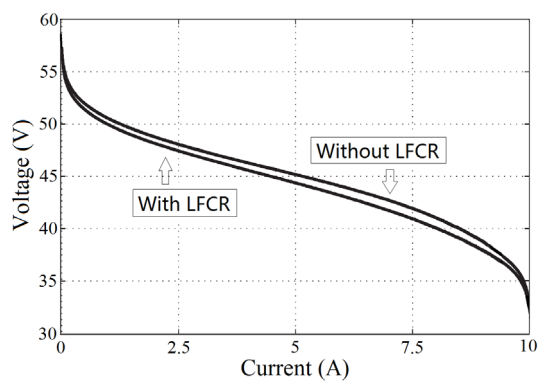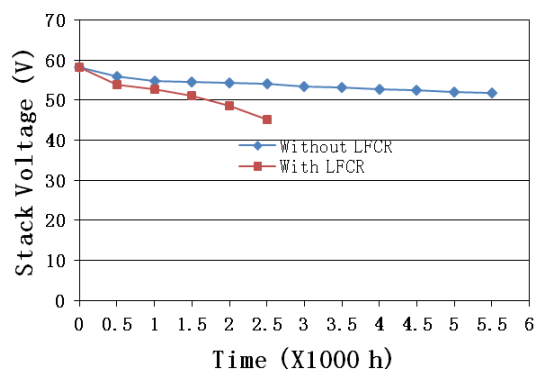
11
12   (a)   (b)
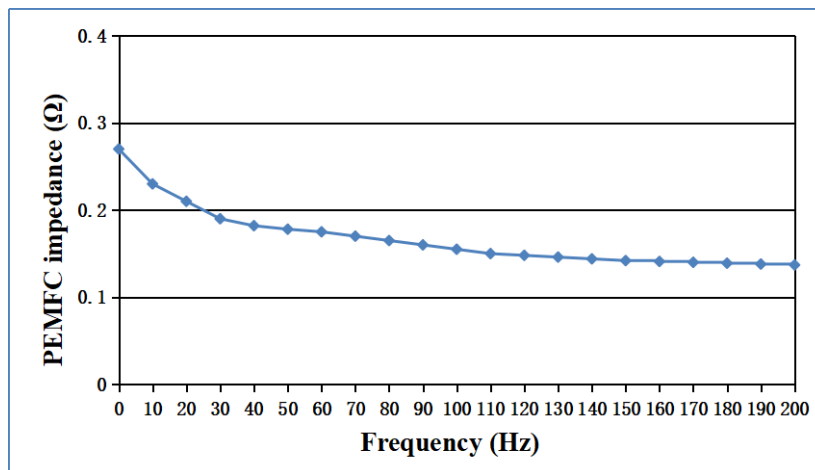
(c)

Fig. 4 — Characteristic charts of PEMFC stack with LFCR and without LFCR:
(a) performance, (b) lifetime, and (c) impedance variation.

4. A review on mitigation technologies of LFCR

As previously mentioned, because the FC is a high current low voltage device, its LFCR becomes a poignant problem for the DC/DC conversion and/or DC/AC inversion design [2, 24]. It is necessary to limit the LFCR within 5% of normal rated value of input current and to ensure the output performance of FC. The USA National Energy Technology Laboratory suggests that the 100 Hz or 120 Hz current ripple should be lower than 15% and the 50 Hz or 60 Hz current ripple should be lower than 10% when the load changes from 10% to 100% [25]. Therefore, to acquire an in-depth understanding in the influences of current ripple and harmonics on an FC, three forms of main topologies and control strategies of mitigating the ripple current have been presented and reviewed, which are the passive compensation methods, active compensation methods, and passive and active hybrid compensation methods [26].

To reduce the undesired LFCR, a lot of research works have been investigated with three types of topological and mitigation approaches as follows. Furthermore, in practical FC PCS applications, because of the sizes and cost of mitigation control devices for LFCR, the research results are inclined to the active compensation approaches to obtain a high voltage boost ratio and high power efficiency.

4.1. Passive compensation approaches

Passive compensation methods are some input current ripple cancellation networks composed of the inductors, filter capacitors, or supercapacitors (SCs) in DC bus sides of a DC/DC conversion based on a basic boost converter [17, 27], or applying the input and output inductance and capacitance series resonance circuits [28], and the current ripple compensation of parallel and multiple boost converter. However, in spite of that the current ripple percentage has been mitigated, raising the size and space of the power conversion devices may result in lower efficiency in PC PCS.

The overview in each reference in this section is shown in Table 1. In the table, it is often common to necessitate a component increase to mitigate the effects of LFCR on FC and to obtain other benefits. Therefore, when choosing a power converter type of passive compensation methods, the designer must establish the exact requirements of FC PCS to determine the most appropriate design.

In the single-stage power conversion, [29-32] used the three-phase boost inversion, single-phase boost inversion, and boost-buck inversion topologies respectively with the

boosting and inversion functions. On the one hand, the boost inverter output voltage is the voltage control mode and the DC/DC bidirectional converter was the current control mode. On the other hand, the proposed system contains an additional battery as the energy storage and a DC/DC bidirectional converter for supporting momentary load changes. Because the load energy is supplied by the battery, the effect of such LFCR is minimized.

In the multiple-stage power conversion, the parallel boost converters using the SCs for the LFCR for a high frequency ripple could ensure efficient energy operation of FC stack, and to minimize the output current ripple of FC stack [33]. In [34], a two-stage PCS includes a single-phase full-bridge inverter and a switched capacitor DC/DC boost converter. To improve the FC hybrid electric vehicle (EV) application, a new DC/DC converter topology was proposed [35], which is defined as floating interleaving boost converters. Compared with the conventional boost converter, although containing the passive components, such as the inductance and capacitance, it has the advantages of lower volume and weight, mitigation of LFCR, and improving the efficiency and transfer boost ratio of the system. In Table 1, a two-stage three-bridge isolated bidirectional DC/DC conversion and DC/AC inversion was presented [36]. A two-stage capacitor division and synchronizing operation can reduce the LFCR currents of the high voltage source through linking the capacitor. To mitigate the input LFCR, a parallel input and series output DC/DC boost converter was adopted [37], and two capacitors in series were linked on the output side for achieving a higher voltage step-up. The

1 experimental results validated the feasibility and suitability of the proposed topology for

2 the fuel cell electric vehicle (FCEV), in which the DC/DC converter maximum and

3 minimum efficiencies are 96.62% and 94.14%, respectively.

4
5
6
7
8
9
10
11
12
13
14
15
16
17
18
19
20
21
22
23
24
25
26
27
28
29
30
31
32
33
34
35
36
37
38
39
40

1 **Table 1**

2 Summary of passive compensation approaches in the literature.

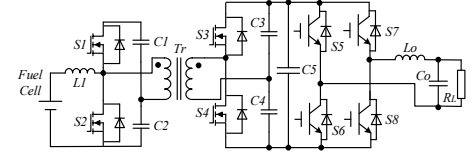| Refs.	Circuit Configuration	Topologies/ Control strategies	Application/ Current ripple	Advantages/ Limitations
[29]		Current-mode-controlled bidirectional boost inverter with back-up unit Double loop control: Inner current and outer voltage	FC energy system 4.5%	Single-stage power conversion
[30]		Current-mode-controlled three-phase boost inverter with back-up unit Double loop control: Inner current and outer voltage	FC energy system Not mentioned	Single-stage power conversion
[31] [32]		Buck-boost inverter Double voltage control	FC energy system 2.0%	Single-stage power conversion
[33]		Multi-boost converter Differential flatness control: energy and current control	FCEV Not mentioned	High efficiency
[34]		Switched capacitor boost converter Proposed voltage and current control: FPGA-based adaptive control	PEMFC energy system 3.0%	Digital control Large size

3
4
5
6

1 Table 1(continued)

Refs.	Circuit Configuration	Topologies/ Control strategies	Application/ Current ripple	Advantages/ Limitations
[35]		N-phase floating-interleaving boost converter (FIBC) Sliding mode control	FCHEV 1.5% (6-phase) 6.5% (4-phase)	Low volume, weight, and high boost ratio
[36]		Two-stage isolated/bidirectional DC/DC converter Buck-boost control modes with zero-voltage switching (ZVS)	A 2-kW prototype converter Not mentioned	Zero-voltage switching Large size
[37]		Input-parallel and output-series DC/DC boost converter Continuous and discontinuous conduction mode (CCM and DCM)	FCEV < 20%	High efficiency

2

4.2. Active compensation approaches

4   Passive compensation approaches would cause the power converters higher cost,

5 larger size and less efficiency, thus the recent researches have focused on the active

6 compensation approaches, which have different types of topologies and mitigation

7 control strategies.

8   According to [26, 38], there are two main categories in the active compensation

9 methods: the power conversion self-regulating approach [24] and the current ripple

injecting control approach [39]. In these approaches, the mitigation strategies have been conducted using different control technologies, such as the proportional integral (PI) control technology, waveform control technology, proportional resonant (PR) control technology, neural network control (NNC) technology, sliding mode control (SMC) technology, and other control strategies, which are reviewed as follows.

4.2.1. Topologies and design of power electronics

As mentioned above, to reduce the effect of LFCR on an FC, the power converter topological designs may also cause the increase of the cost and size in the power converters due to the cost of extra components as the passive compensation approaches. A low component number and high boost abilities are necessitated for PEMFC application, so the high step-up converter and high efficiency are the best choice. Therefore, adding a boosting capability based on the conventional power converters, applying the digital signal processor (DSP), and having a high efficiency through the implementation of control technologies for sacrificing the power density and device number, are the latest research trends in the developments of FC power electronics design, and advanced control methods to improve the lifespan and the robustness of FC PCS.

The overview in the references in this section is shown in Table 2. In the overview, multiple types of topologies designs for the active compensation methods are examined.

1 Table 2 reveals also some of the advantages and limitations of the power converter

2 topologies.
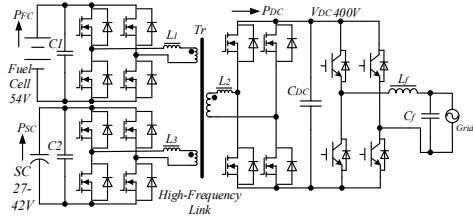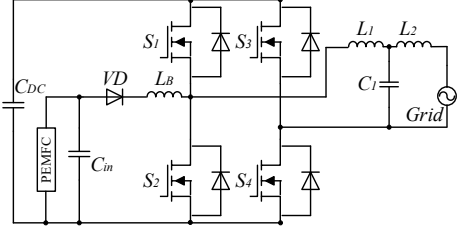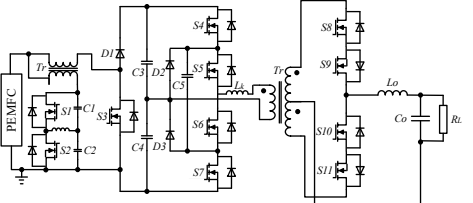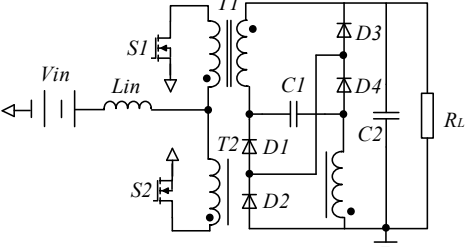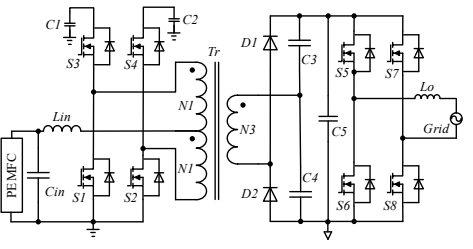
3
4
5
6
7
8
9
10
11
12
13
14
15
16
17
18
19
20
21
22
23
24
25
26
27
28
29
30
31
32
33
34
35
36
37
38
39
40
41
42
43
44
45
46
47
48
49
50
51
52
53
54
55
56
57
58
59
60
61
62

Table 2
Summary of the topologies and design of power electronics in the literature.

Refs.	Circuit Configuration	Topologies/ Control strategies	Application/ Current ripple	Advantages/ Limitations
[40]		Phase-shifted, cascaded boost, series connected, and push-pull converter Not mentioned	FC PCS 18%(PSB), 20%(CBP), 28%(SCC), 31%(PP)	General analysis of LFCR
[41] [42] [43]		Multi-input dual-active-bridge (DAB) DC/DC converter Current and voltage PI control; frequency-adaptive proportional-resonant (PR) control	FC renewable energy systems Reduced by 85.5%	Bidirectional power flow
[44]		High power factor (PC) frond-end boost converter Average current and voltage PI control	FC-powered UPS System Less than 7%	Simple topology and control
[45]		Frond-end boost converter and single-phase inverter Current and voltage PI control	two-stage power converter 2.98%	Low LFCR
[46]		Active clamp ZVC flyback-forward converter Average current mode and voltage PI control	FC power generation system Below 1.5%	High efficiency Low LFCR
[47]		Back-boost converter Current control	FC power converter 4.5%	Simple topology and control

Refs.	Circuit Configuration	Topologies/ Control strategies	Application/ Current ripple	Advantages/ Limitations
[48]		Three port bidirectional DC/DC converter and grid-interfacing inverter Active current estimator, current PI control, and phase-locked-loop (PLL)	FC-powered UPS system No mentioned	Bidirectional converter More switches
[49]		Single-stage and boost-voltage grid-conditioned inverter Boost inductor current and resonant control	FC power generation system 1.6%	single-stage circuits Lower LFCR
[50]		Current-fed dual-half-bridge (DHB) DC/DC converter Proposed pulsation power decoupling control	FC PCS 2.55%	Low LFCR, two-stage circuits
[51]		Zero-ripple boost converter, multilevel high-frequency inverter and line frequency switched cycloconverter (LFSC) Current and voltage PI control	FC PCS 5% to 97%	Small size, and cost
[52]		A novel current-fed boost converter with ripple reduction (BCRR) Control modes of the BCRR	High voltage conversion applications No mentioned	Simple circuits High boost ratio
[53]		Current-fed resonant push-pull converter with active clamp circuits and a full-bridge inverter Control modes of proposed step-up converter	FC PCS Less than 2%	High efficiency, Low LFCR, Excellent control strategy

Table 2 (continued)

Refs.	Circuit Configuration	Topologies/ Control strategies	Application/ Current ripple	Advantages/ Limitations
[54]		A novel parallel-series full bridge (PSFB) DC/DC converter Input current control	FC PCS Less than 3%	Novel DC/DC conversion, Lower LFCR
[55]		DC/DC converter (two boost converters and a voltage doubler) and DC/AC inverter (dual-back converter and full-bridge inverter) Input current control for DC/DC converter and direct double closed-loop control for DC/AC inverter	Grid-connected FC power generation system 4.2%	High boost ratio, Novel configuration, Lower LFCR
[56]		A new single-switch non-isolated DC/DC converter Continuous conduction mode and discontinuous inductor conduction mode (DICM)	FC PCS Near-zero	Simple circuits, High boost ratio, Near-zero LFCR
[57]		Single-phase pulse width modulated and isolated inverter Current and voltage control with DC active filter function	Grid-connected FC System Reduced 20%	Low number of switching devices, Common mode

Ref. [40] compared analytically and discussed the LFCR with different conversion topology, such as the cascaded boost and push-pull converter (CBP), phase shifted boost and push-pull converter (PSB), series connected converters (SCC), and cascaded push-pull DC/DC converter (PP) in FC PCS applications. The parameters of peak switching currents and the percentage of peak to DC level of LFCR were analyzed using

these conversion topologies in this system. Refs. [41-43] presented a multiple input

bidirectional dual active bridge (DAB) DC/DC converter with shared secondary

half-bridge unit and a systematic derivation of four basic modes of output impedance.

Using the double PI control and adaptive frequency PR control respectively and the

minimized impedance design for the harmonic currents flow in the battery branch can

help improve the system dynamic response and harmonic absorption. Ref. [44]

proposed the front-end converter with an integrated power factor correction (PFC) and

an additional dedicated DC/DC converter in a PEMFC PCS. The PEMFC replacing the

battery banks was applied in a UPS system as an energy storage unit, dispelling the

common shortcomings related to the performance and lifetime of PEMFC. Similarly,

[45] designed a two-stage front-end boost converter with PI control, based on series and

parallel feedback control technology, which increases the boost converter output

impedance, and decreases the LFCR in this converter.

Ref. [46] presented an interleaved soft switching flyback-forward DC/DC

conversion and a full-bridge inversion with a high power efficiency and high voltage

gain. Ref. [47] proposed an auxiliary type of power converter, which operated as an

active filter to supply the LFCR required by the load and PCS. It can improve the

typically slow dynamic response of FC stack, and in turn optimize the system operation.

Ref. [48] proposed a line-interactive FC-UPS system. In a three-port bidirectional

converter, an FC and an SC were connected to a grid-interfacing inverter, in which an

active filtering device was integrated into the hybrid FC/SC system. Moreover, the SC

can not only used as both an active and a passive energy storage, but also buffer the periodical LFCR in the requested power. Ref. [49] presented a new single-stage boost voltage inversion with a boost current inductance in a grid-connected system, which can effectively reduce the LFCR in the output current of FC. Ref. [50] proposed a current-fed dual half-bridge (CFDHB) DC/DC conversion with a power pulsation decoupling control strategy. Low LFCR can be achieved since the conversion as the load of PCS was linked to the FC system. Ref. [51] proposed an FC PCS system, which comprises a zero ripple filter and boost converter followed by soft switches and multilevel high frequency inverter and a single-phase cycloconverter in the stationary application. Ref. [52] proposed a novel current-fed boost converter with LFCR mitigation method, which features a high voltage gain with small transformer turn ratio and minimum components. Ref. [53] proposed a push-pull DC/DC conversion using the current-fed resonant and active clamp circuits and a full-bridge DC/AC inversion in FC PCS, indicating a high voltage boost ratio and high power efficiency. Ref. [54] presented a new parallel/series full-bridge (PSFB) DC/DC conversion for improving its phase shifting value, which can mitigate the LFCR suppressing applied on PCS.

Ref. [55] presented a novel power electronic interface in the grid-connected system. A double voltage topology was employed to configure the DC/DC conversion to obtain a high voltage step-up. Ref. [56] proposed a new high voltage boost ratio non-isolated single-switch DC/DC converter for reducing semiconductor voltage stress. The near zero LFCR can be achieved at the input DC bus side for improving the lifespan of FC

1 stack. Ref. [57] proposed an LFCR reduction method to realize a DC active filter

2 function without increasing the number of switching devices.

3

4 4.2.2. Waveform control

5 Refs. [46-49] proposed a waveform control strategy that can reduce the LFCR of

6 DC/AC boost inverters in a single conversion stage grid-connected system, as shown in

7 Fig. 5, which is a boost-type differential inverter.
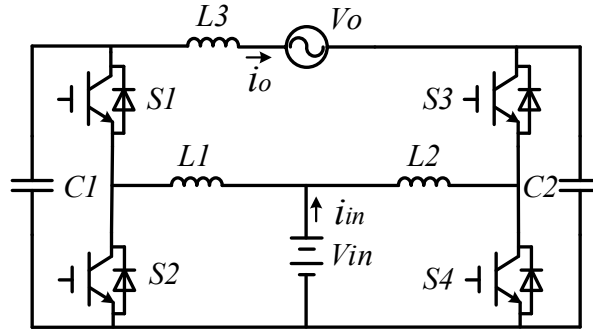
8

9 **Fig. 5** — Configuration of a differential boost inversion [58-61].

10 If the amplitude B is determined by:

11 $$B = \frac{V_{max}}{8V_d \omega C}\sqrt{I_{max}^2 + \omega^2 C^2 V_{max}^2 / 4}$$ (12)

12 and the phase angle φ is determined by:

13 $$\varphi = \frac{\pi}{2} - \arcsin\frac{I_{max}}{\sqrt{I_{max}^2 + \omega^2 C^2 V_{max}^2 / 4}}$$ (13)

14 the input current of low frequency component at 2ω is:

15 $$i_{in}(2\omega) = \frac{\frac{1}{2}V_{max}^2 \omega C \sin(2\omega t) - V_{max}I_{max}\cos(2\omega t)}{2V_{in}}$$
$$+ \frac{8V_d B \omega C \cos(2\omega t + \varphi)}{2V_{in}} = 0$$ (14)

16 4.2.3. Proportional resonant (PR) control

Refs. [62, 63] proposed a swinging bus technology in an FC stand-alone application, and a natural switching surface (NSS) was used to operate DC/AC inversion with very large input voltage swing, as depicted in Fig. 6. To explain the superior function of the NSS, a comparison was performed to a PR controller. Moreover, the small film capacitors instead of electrolytic ones were employed in the single-phase inversion in FC PCS application.
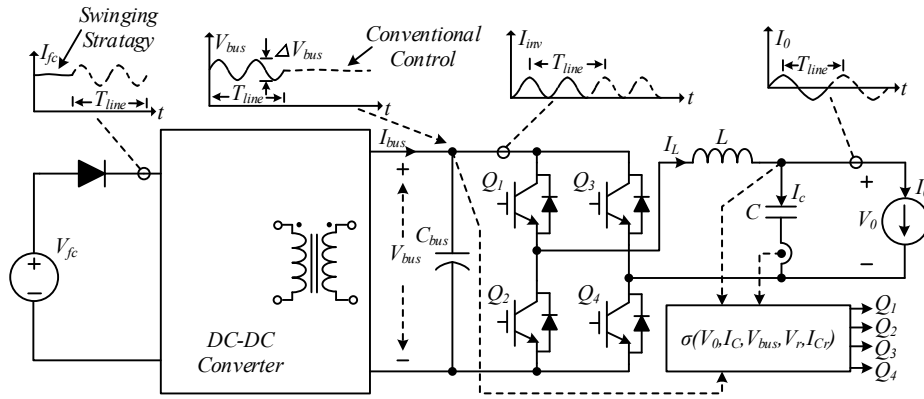
Fig. 6 — Schematic diagram of PCS with a swinging bus technology [62, 63].

The switching surfaces $\sigma_i (i = 1, 2, 3)$ ruling the behaviour of the swinging bus inversion are expressed as:

$$\sigma_1 = i_{Crn}^2 + (v_{rn} - v_{busn})^2 \tag{15}$$

$$\sigma_2 = i_{Crn}^2 + v_{rn}^2 \tag{16}$$

$$\sigma_3 = i_{Crn}^2 + (v_{rn} + v_{busn})^2 \tag{17}$$

where i_{Crn} is the current reference of normalized output filter capacitor (A), v_{rn} the normalized reference output voltage (V), and v_{busn} the normalized DC bus side voltage (V).

Ref. [64] proposed a direct LFCR control in a single-phase high PCS, which can achieve lower LFCR without using large electrolytic capacitors, as shown in Fig. 7. A

1　PR controller was also developed to eliminate the LFCR disturbance introduced by the

2　load of single-phase DC/AC inversion, and to achieve an extra high voltage step-up at

3　designed resonant frequency.

4
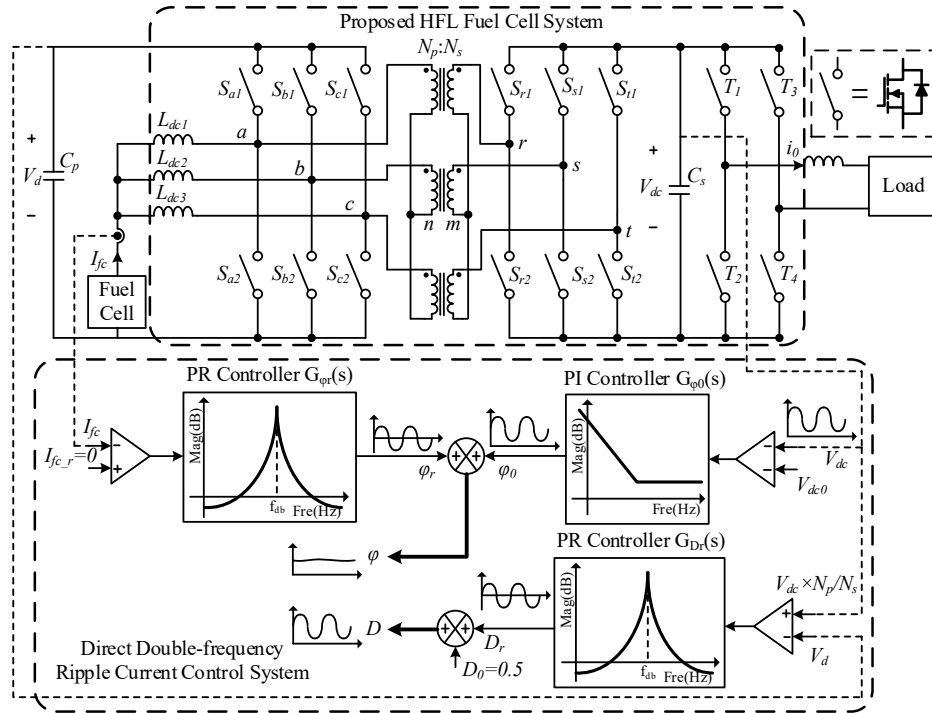
5　**Fig. 7** — Proposed diagram of direct LFCR control system [64].

6　4.2.4. Intelligent and advanced control technology applications

7　Refs. [26, 65] proposed a two-stage power converter with a dual active low

8　frequency ripple control circuit (DALFRCC) and an active LFCR circuit respectively,

9　as depicted in Fig. 8, in which a linear adaptive neural network was applied as a neural

10　filter for generating the compensation current, and an SMC was used to regulate the

11　ripple control circuit to inject a suitable compensation current into the high voltage side

12　in the PCS. Ref. [66] proposed a new FC hybrid power source topology to mitigate the

13　LFCR of FC PCS and realize the maximum power point tracking (MPPT) function, as

14　depicted in Fig. 9, in which the LFCR reduction method was based on active

1   compensation control strategy. Two methods were used to design the nonlinear control

2   law. One is the simulation trials to help drawing the characteristic of mitigation ripple

3   ratio through the current ripple of FC; the other is the fuzzy logic controller, in which

4   the ripple factor could be reduced up to 1%.
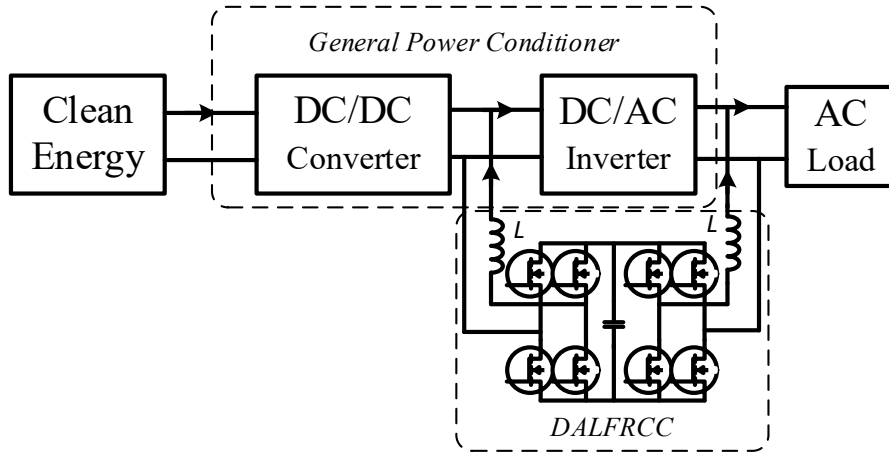
6   **Fig. 8** — Structure chart of the general PCS with DALFRCC [26, 65].
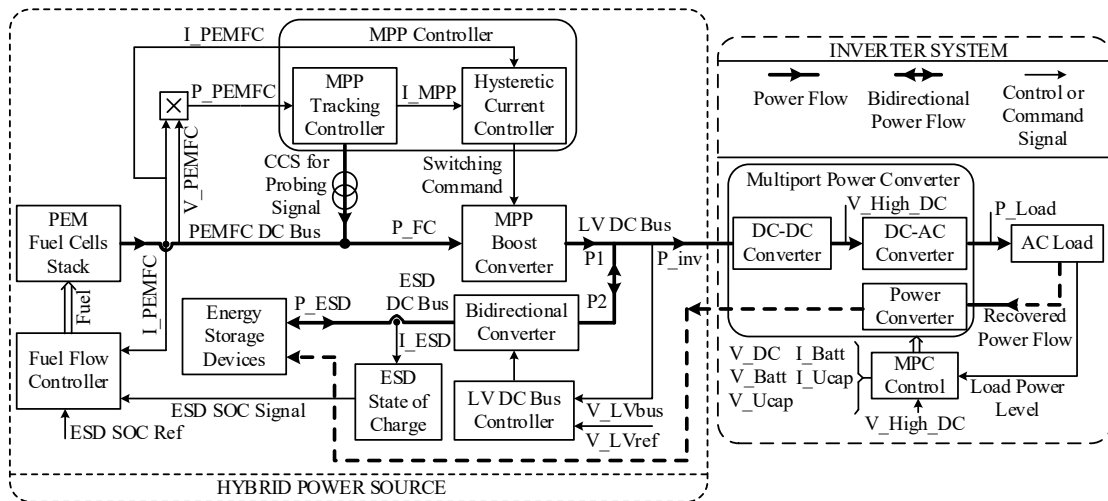
8   **Fig. 9** — Hybrid power source topology operating in MPPT of PEMFC stack [66].

9   Ref. [18] proposed a new adaptive sliding mode control for a two-stage

10 DC/DC/AC front-end boost converter to reduce the influence of LFCR without

11 impacting the dynamic performance, as depicted in Fig. 10, which can reduce the ripple

1   component at battery input, and the control can form the output impedance of the

2   proposed boost converter.
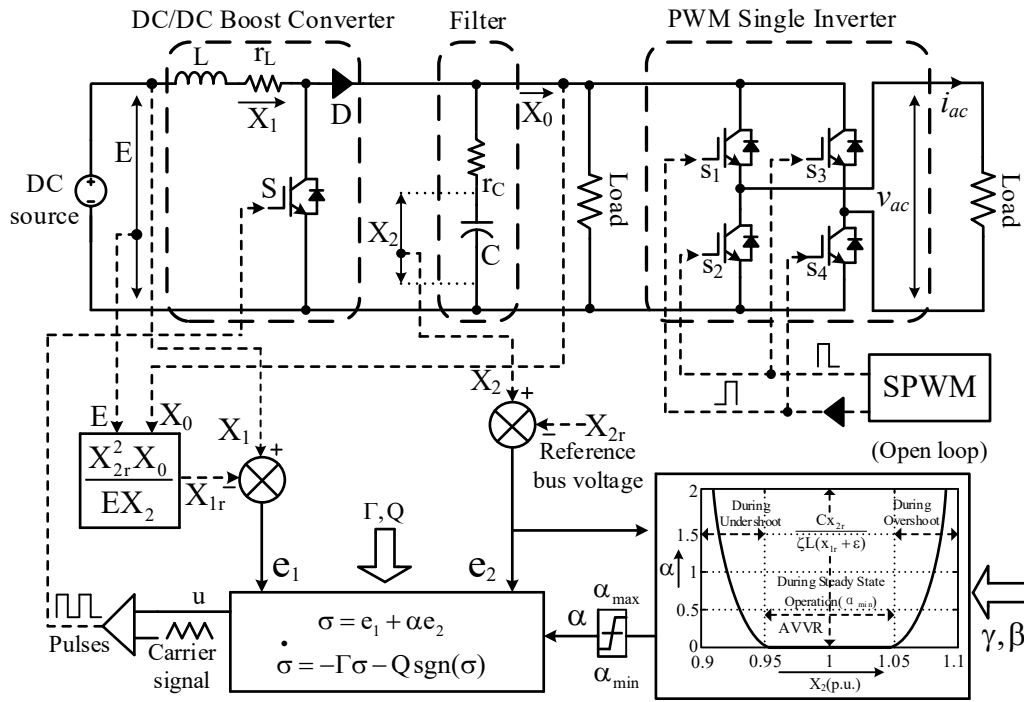
3

4   **Fig. 10** — A two-stage DC/DC/AC converter with adaptive SMC approach [18].

5   4.2.5. Other control strategies

6   Ref. [10] presented the front-end DC/DC converter with the load current
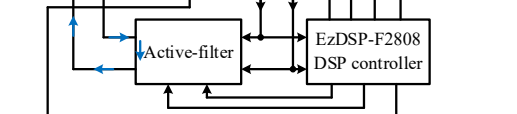
7   feedforward, to reduce the LFCR, as depicted in Fig. 10.

8
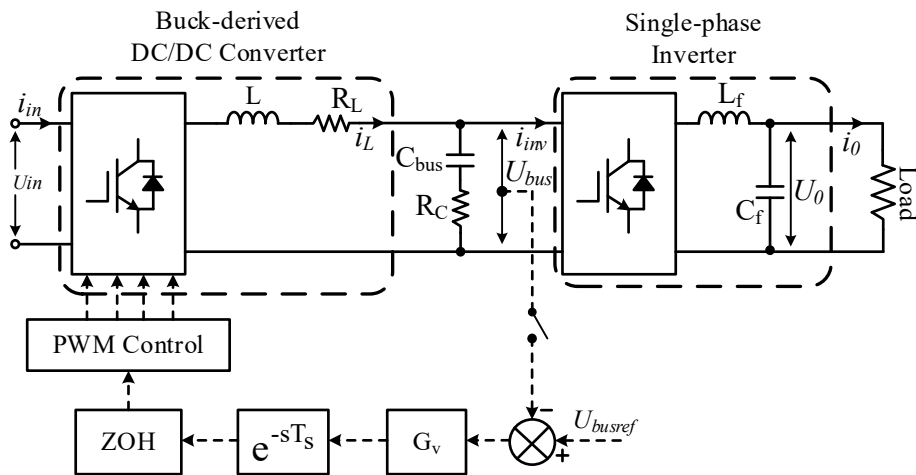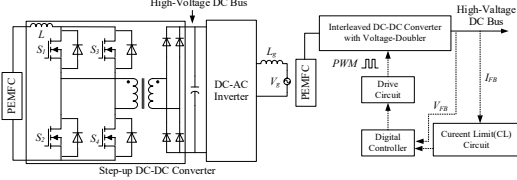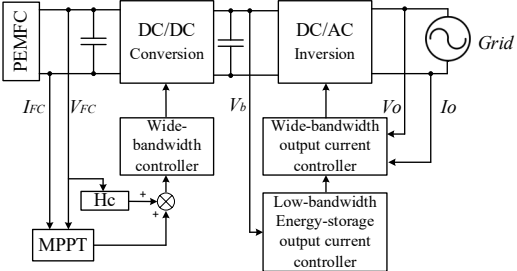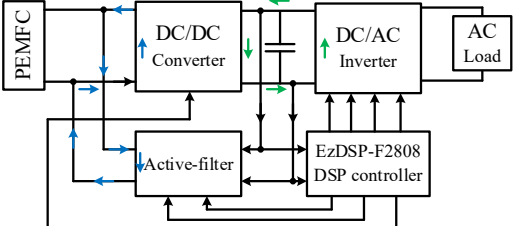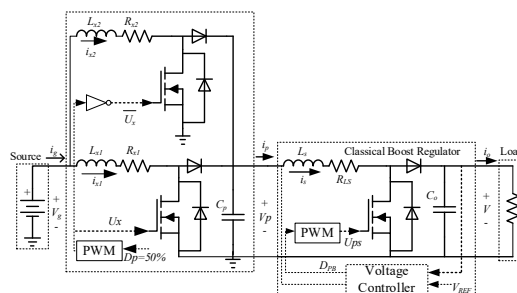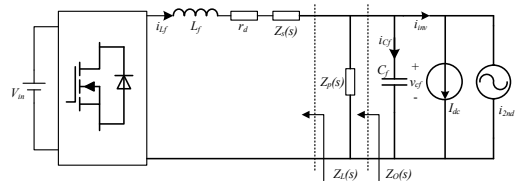
Fig. 11 — A two-stage single-phase inverter with load current feedforward [10].

The overview in the references in this section is shown in Table 3. As seen in the table, based on the traditional boost converter, adopting different control strategies, such as the digital-controlled control, current-fed control, active clamp control circuits, and pre-regulator control, the proposed power converters in mitigation of the LFCR and harmonics can realize the high boost ratio and high efficiency.

1 **Table 3**

2 Summary of other control strategies in the literature.

Refs.	Circuit Configuration	Topologies/ Control strategies	Application/ Current ripple	Advantages/ Limitations
[67]		Current-fed full-bridge DC/DC converter with voltage doubler and active clamp circuits Digital-controlled current and voltage control	PEMFC PCS Not mentioned	High efficiency, High boost ratio
[68]		Boost full-bridge DC/DC converter with proposed active ripple reduction network Wide-bandwidth voltage and current control with MPPT function	Grid-connected FC System 1.2%	Low LFCR, Long lifetime of FC
[69] [70]		Boost converter with active filter circuits and Full-bridge inverter Active filter control of input current and voltage using DSP	FC PCS Reduced about 50%	DSP digital controller
[71]		Cascaded low ripple voltage doubler pre-regulator and boost regulator converter Pre-regulator control and classical boost control	FCs or photovoltaic systems Reduced 12%	Simple circuits and control strategy
[72]		Buck-derived front-end DC/DC converter BPF-ICFS NF-LCFFS NF-CR+LCFFS VRS	Simple two-stage inverter 1% 5% 3% 5%	LFCR compassion study

3

1 To mitigate the LFCR and raise the FC reliability, a high efficiency and high boost

2 ratio digital-controlled interleaved DC/DC conversion with an active clamp circuit in

3 PEMFC application was proposed in [67]. Ref. [68] proposed a two-stage single-phase

4 inversion in FC PCS application and a novel control strategy, to mitigate the LFCR of

5 FC and guarantee the FC reliability. It can increase the FC lifespan, and avoid

6 unnecessary consumption of reactants and high mechanical stress of the membrane.

7 Refs. [69, 70] proposed an active filtering method to remove the LFCR drawn from the

8 FC in a single-phase and three-phase FC systems, respectively, which provides an

9 alternate path to prevent the 100 Hz or 120 Hz LFCR from flowing through the FC. Ref.

10 [71] proposed a classical boost converter with the series connecting of LFCR voltage

11 double pre-controller for improving the efficiency of PCS and reducing the LFCR,

12 which is suitable for current ripple sensitive PGS, such as FC or photovoltaic systems.

13 Ref. [72] took the front-end buck-derived DC/DC converter, which can realize the

14 implementation of the virtual impedance. Based on the theoretical analysis and

15 experimental verification, a comparative study was conducted on different control

16 schemes, such as the bandpass filter incorporated inductor current feedback scheme

17 (BPF-ICFS), bandpass filter incorporated capacitor voltage feedback scheme

18 (BPF-CVFS), notch filter inserted current mode control scheme (NF-CMCS), notch

19 filter inserted load current feedforward scheme (NF-LCFFS), notch filter inserted

20 current reference plus load current feedforward scheme (NF-CR+CFFS), and virtual

21 resistor control scheme (VRS).

1 **4.3. Passive and active hybrid compensation methods**

2   Regarding these methods, a hybrid filter topology with a passive stage and an

3 active stage was presented in [73], which can be implemented in any renewable energy
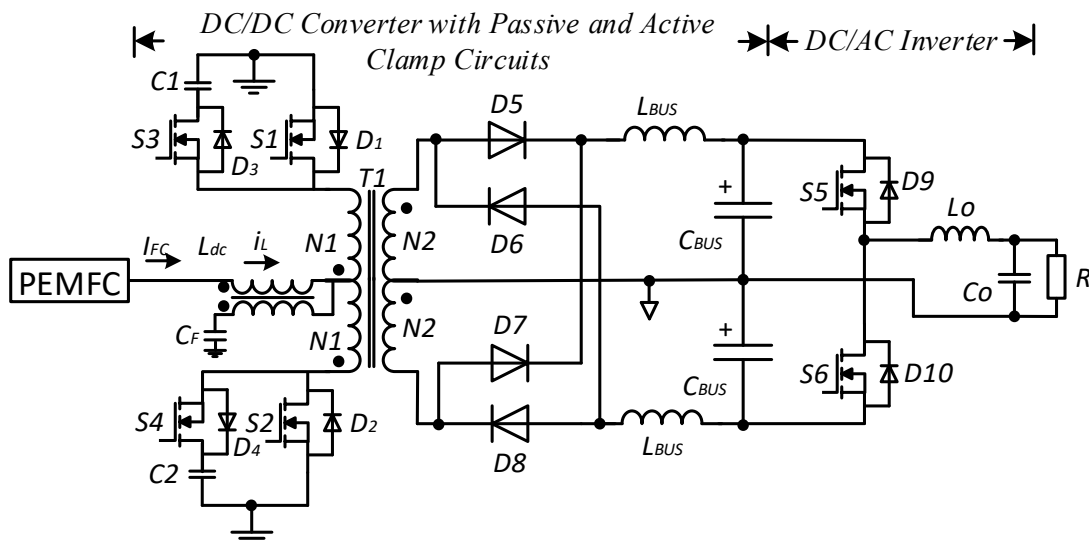
4 system.

5   Based on our researches in this field, a case study in this method will also be

6 designed and discussed in Section 5.

7

8 **5. Design and experimental of a passive and active hybrid compensation method**

9 **5.1. Design of digital current ripple controller**

10   In this paper, as a case study, to mitigate the LFCR and harmonics and not to

11 increase the size and cost in a PEMFC PCS, a push-pull DC/DC conversion with

12 current-fed resonant function and active clamp circuits is conducted, as depicted in Fig.

13 12.

14
15   **Fig. 12** — PEMFC-UPS system with passive and active hybrid compensation circuits.

1   In Fig. 12, the DC/DC converter contains the main power switches S1 and S2, the

2   auxiliary clamping power switches S3 and S4, the anti-parallel diodes D1 and D2, the

3   active clamping diodes D3 and D4, and the active clamping capacitors C1 and C2. The

4   operation principle of the push-pull DC/DC converter on the condition of the successive

5   current is:

6    $$\frac{V_{BUS}}{V_{FC}} = \frac{2n}{1 - D_c} \tag{18}$$

7   where $n = N_1/N_2$, D_c is the basic duty ratio of output control for regulating the

8   voltage of DC bus side, V_{BUS} the voltage of DC bus side (V), and V_{FC} the voltage of

9   PEMFC (V).

10   According to the designed DC/DC converter, a DSP for output voltage $\pm V_{BUS}$ and

11   reducing LFCR is adopted to regulate the total duty ratio D_{out}, including the duty ratio

12   control of the DC bus side voltage and the duty ratio control of mitigating the LFCR

13   and harmonics, which is:

14    $$\frac{v_{BUS}(t)}{V_{FC}} = \frac{2n}{1 - D_{out}} = \frac{2n}{1 - (D_c + D_r)} \tag{19}$$

15   where D_r is a ripple mitigation control duty ratio. Eq. (19) can be rewritten as:

16    $$D_r = (1 - D_c) - 2n \cdot \frac{V_{FC}}{v_{BUS}(t)} \tag{20}$$

17   There is:

18    $$v_{Bus}(t) = V_{Bus}\left[1 + \frac{V_0 I_0}{2\omega C_{Bus} V_{Bus}^2} \sin(2\omega t + \varphi)\right] \tag{21}$$

19   where C_{Bus} is the filtering capacitors of DC bus side (V).

Substituting (18) and (21) into (20), there is:

$$D_r = \frac{2nV_{FC}}{V_{BUS}} \cdot \frac{\dfrac{V_0 I_0 \sin(2\omega t + \varphi)}{2\omega C_{BUS} V_{BUS}^2}}{1 + \dfrac{V_0 I_0 \sin(2\omega t + \varphi)}{2\omega C_{BUS} V_{BUS}^2}} \tag{22}$$

Letting $1 + \dfrac{V_0 I_0 \sin(2\omega t + \varphi)}{2\omega C_{BUS} V_{BUS}^2} \approx 1$, Eq. (22) becomes an open-loop control mode for

active compensation function, which is:

$$\begin{aligned} D_r &= \frac{nV_{FC}}{V_{BUS}} \cdot \frac{V_0 I_0 \sin(2\omega t + \varphi)}{\omega C_{BUS} V_{BUS}^2} \\ &= k V_{FC} I_0 \sin(2\omega t + \varphi) \end{aligned} \tag{23}$$

where $k = \dfrac{nV_0}{\omega C_{BUS} V_{BUS}^3}$.

In practical PEMFC UPS application, the designed coupled inductances for passive compensation function are $L_{ac} = 23.0\,\mu H$, $L_{dc} = 52.5\,\mu H$, the turn ratio $\alpha = N_{dc}/N_{ac} = 11/7$, and $C_F = 10\,\mu F$. Therefore, when $u_{ac} = \alpha V_{FC}$, the almost zero-ripple current condition can be expressed as:

$$\frac{di_{FC}}{dt} = \frac{1}{L_{dc}(1 - k^2)} \left(V_{FC} - k\sqrt{\frac{L_{dc}}{L_{ac}}} \cdot u_{ac} \right) \tag{24}$$

Fig. 13 shows the DSP TMS320F2406 push-pull DC/DC converter controller, following an electrically programmable logic device (EPLD). All the control functions are fully executed in software of DSP [74].
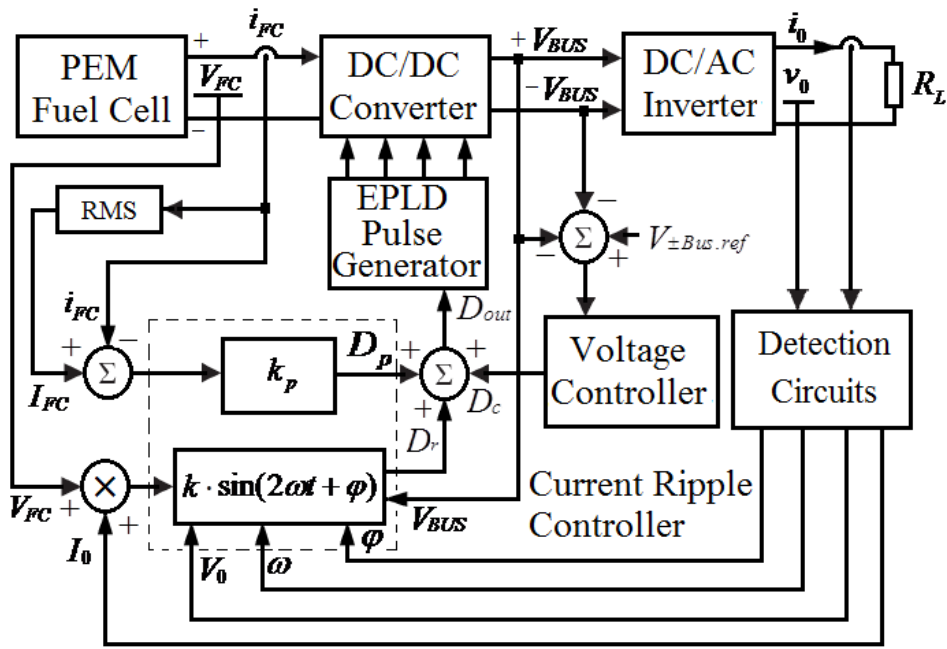
Fig. 13 — Construction diagram of LFCR reduction controller in UPS system.

5.2. Experimental setup

The experimental setup contains a 700 W high frequency UPS system, a 300 W 36 V of PEMFC PGS, a data-acquisition test system, and lead-acid batteries. In the PEMFC PGS, the hydrogen and air mass flows are controlled by F-201C-GAS-22V and F-112AC-GAS-22V (Bronkhorst). The humidity and temperature measurement devices of air and hydrogen are the type of hydrotransmitter HD2008TV1 (Delta OHM), and the pressure transmitter is the AUS EX 1354X (Burkert) between the inlets of cathode and anode. A LA55-P and a LV25-P are used to measure the current and voltage of PEMFC. The data-acquisition system can record all the physical parameters in the PEMFC PGS and PCS system [75].

5.3. Experimental results

There are severe LFCR and harmonics in DC bus side, as depicted in Fig. 14(a), The figure indicates the voltage and current waveforms of a 300 W 36 V PEMFC without any LFCR reduction strategies of DC/DC conversion and DC/AC inversion in PEMFC PGS, in which a 100 Hz of large current ripple exists. As a case study, when the peak to peak current ripple value ($I_{FC_{pp}}$) of PEMFC is 2.0 A, and the input current average value ($I_{FC_{ave}}$) of PEMFC is 8.218 A, the current ripple percentage (CR%) of PEMFC can be computed as:

$$Current\ ripple\ (CR\%) = \frac{I_{FC_{pp}}}{I_{FC_{ave}}} \times 100\% = \frac{2.0\ A}{8.218\ A} \times 100\% = 24.3\,\% \tag{25}$$

Using the proposed digital-controlled LFCR reduction control strategy in the push-pull DC/DC with active clamp circuits for PEMFC PCS application, as shown in Fig. 12, the experiment and computing results show that the current average value of PEMFC is 8.198 A and the peak to peak current ripple value of PEMFC is 0.098 A. The current ripple and voltage ripple percentages of the PEMFC can be mitigated to about 1.2 % and 4.8%, respectively, as shown in Fig. 14(b). Therefore, the digital-controlled LFCR reduction controller in a push-pull DC/DC converter with active clamp circuits could effectively reduce the LFCR.

(a)   (b)
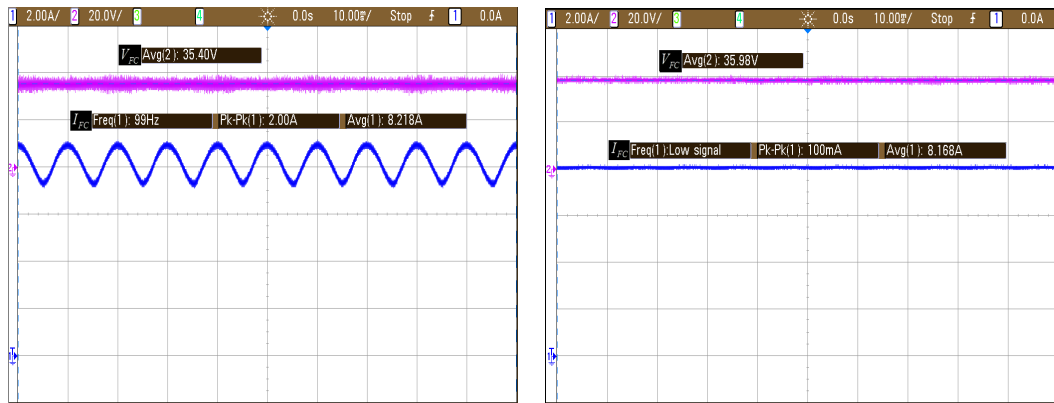
Fig. 14— Current and voltage waveforms of PEMFC in an UPS system: (a) with LFCR and harmonics; (b) with a digital-controlled push-pull DC/DC converter with active clamp circuits.

6. Conclusion and research trends

The construction, types, application and electrical characteristics of PCS controlling the LFCR in PEMFC PCS application are reviewed and discussed in this paper. Firstly, the basic structures of PEMFC PCS and the performance effect of LFCR on PEMFC are analyzed and validated. Secondly, the three types of LFCR reduction methods and their control and diagnosis strategies are reviewed. Then, the passive and active hybrid method is designed as a case study. Finally, the experimental results show that the proposed mitigation control strategy has better performance on reducing the input current ripples, cost and size.

According to the summary and review results, the current research and development trends in the power electronics for extending lifespan and robustness of FC PGS are as follows: (1) Influence of power converter with LFCR, current ripples, and harmonics on FC degradation and lifetime; (2) Novel topologies and control strategies of power electronics to enhance the lifetime and reliability for FC PCS; (3)

Optimal power electronics for reduction and elimination of LFCR and harmonics in FC

PCS; and (4) Reliability analysis of FC power conversion methods for preventing FC

degradation.

Acknowledgments

References

[1] Gemmen RS. Analysis for the effect of inverter ripple current on fuel cell operating

condition. J Fluids Eng. 2003; 125(3): 576-85.

[2] Mazumder SK, *et al.* Solid-oxide-fuel-cell performance and durability: resolution of

the effects of power-conditioning systems and application loads. IEEE Trans Power

Electron 2004; 19(5):1263-78.

[3] Gerard M, Poirot-Crouvezier JP, Marie-Cecile Péra DH. Ripple current effects on

PEMFC aging test by experimental and modeling. Fuel Cell Science and Technology

2011; 8(2): 021004 (5 pages).

[4] Wahdame B, *et al.* Impact of power converter current ripple on the durability of a

fuel cell stack. 2008 IEEE International Symposium on Industrial Electronics.

Cambridge, England, 30 June-2 July 2008, p. 1-5.

[5] García-Vite PM, Soriano-Rangel CA, Rosas-Caro JC, Mancilla-David F. A DC/DC

converter with quadratic gain and input current ripple cancelation at a selectable duty

cycle. Renewable Energy 2017; 101: 431-36.

[6] Sha DS, Xu YX, Zhang JK, Yan Y. Current-fed hybrid dual active bridge DC/DC converter for a fuel cell power conditioning system with reduced input current ripple. IEEE Trans Ind Electron 2017; 64(8): 6628-38.

[7] Lu NJ, Yang SF. Tang Y. Ripple current reduction for fuel-cell-powered single-phase uninterruptible power supplies. IEEE Trans Ind Electron 2017; 64(8): 6607-17.

[8] Ramirez-Murillo H, *et al.* An efficiency comparison of fuel-cell hybrid systems based on the versatile buck-boost converter. IEEE Trans Power Electron 2018; 33(2):1237-46.

[9] Naik MV, Samuel P. Analysis of ripple current, power losses and high efficiency of DC/DC converters for fuel cell power generating systems. Renewable and Sustainable Energy Reviews 2016; 59(6):1080-88.

[10] Shi YJ, Liu BY, Duan SX. Low-frequency input current ripple reduction based on load current feedforward in a two-stage single-phase inverter. IEEE Trans Power Electron 2016; 31(11): 9972-65.

[11] Hong P, Li JQ, Xu LF, Yang MG, Fang C. Modeling and simulation of parallel DC/DC converters for online AC impedance estimation of PEM fuel cell stack. Int J Hydrogen Energy 2016; 41(4): 3004-14.

[12] Wang HQ, Gaillard A, Hissel D. Online electrochemical impedance spectroscopy detection integrated with step-up converter for fuel cell electric vehicle. Int J Hydrogen Energy 2019; 44(2): 1110-21.

[13] Mayo-Maldonado JC, *et al.* A novel PEMFC power conditioning system based on

the interleaved high gain boost converter. Int J Hydrogen Energy 2019; 44(24): 12508-14.

[14] Zhang Y, Liu HY, Li J, Sumner M. A low-current ripple and wide voltage-gain range bidirectional DC-DC converter with coupled inductor. IEEE Trans Power Electron 2020; 35(2): 1525-35.

[15] García-Vite PM, et. al. Quadratic buck-boost converter with reduced input current ripple and wide conversion range. IET Power Electron 2020; 12(15): 3977-86.

[16] Zheng YF, Brown B, Xie WH, Li AX, Smedley K. High step-up DC-DC converter With zero voltage switching and low input current ripple. IEEE Trans Power Electron 2020; 35(5): 9418-31.

[17] Li Q, Huangfu Y, Xu LC, Wei J, Ma R, Zhao DD, Gao F. An improved floating interleaved Boost converter with the zero-ripple input current for fuel cell applications. IEEE Trans Energy Conversion 2019, 34(4): 2168-79.

[18] Gautam AR, Gourav K, Guerrero JM, Fulwani DM. Mitigation with improved line-load transients response in a two-stage DC/DC/AC converter: adaptive SMC approach. IEEE Trans Ind Electron 2018; 65(4): 3125-35.

[19] O'hayre RP, Cha S, Colella WG, Prinz FB. *Fuel Cell Fundamentals*, New York: John Wiley & Sons, 2007.

[20] Choi WJ, Howze JW, Enjeti P. Development of an equivalent circuit model of a fuel cell to evaluate the effects of inverter ripple current. J Power Sources 2006; 158(2): 1324-32.

[21] Zhan YD, Guo YG, Zhu JG, Yang B. Comprehensive influences measurement and analysis of power converter low frequency current ripple on PEM fuel cell. Int J Hydrogen Energy 2019; 44(59): 31352-59.

[22] Das HS, Tan CW, Yatim AHM. Fuel cell hybrid electric vehicles: A review on power conditioning units and topologies. Renewable and Sustainable Energy Reviews 2017; 76: 268-91.

[23] Ferrero R, Marracci M, Tellini B. Single PEM fuel cell analysis for the evaluation of current ripple effects. IEEE Trans Instrumentation and Measurement 2013; 62(5):1058-64.

[24] Liu CR, Lai JS. Low frequency current ripple reduction technique with active control in a fuel cell power system with inverter load. IEEE Trans Power Electron 2007; 22(4):1429-36.

[25] NETL. Fuel cell specifications for Future Energy Challenge 2010 Competition, http://www.netl.doe.gov (accessed 2.07.2010).

[26] Wai RJ, Chun YL. Dual active low-frequency ripple control for clean-energy power-conditioning mechanism. IEEE Trans Ind Electron 2011; 58(11):5172-85.

[27] Yu X, Starke MR, Tolbert LM, Ozpineci B. Fuel cell power conditioning for electric power applications: a summary. IET Electric Power Applications 2007; 1(5):643-56.

[28] Malo S, Grino R. Design, construction, and control of a stand-alone energy-conditioning system for PEM-type fuel cells. IEEE Trans Power Electron 2010; 25(10):2496-506.

[29] Jang MS, Agelidis VG. A minimum power-processing-stage fuel-cell energy system based on a boost-inverter with a bidirectional backup battery storage. IEEE Trans Power Electron 2011; 26(5):1568-77.

[30] Jang MS, Agelidis VG. A boost-inverter-based, battery-supported, fuel-cell sourced three-phase stand-alone power supply. IEEE Trans Power Electron 2014; 29(12):6472-80.

[31] Jang MS, Ciobotaru M, Agelidis VG. A single-stage fuel cell energy system based on a buck-boost inverter with a backup energy storage unit. IEEE Trans Power Electron 2012; 27(6):2825-34.

[32] Jang MS, Ciobotaru M, Agelidis VG. A single-phase grid-connected fuel cell system based on a boost-inverter. IEEE Trans Power Electron 2013; 28(1):279-88.

[33] Thounthong P, Pierfederici S, Martin JP, Hinaje M, Davat B. Modeling and control of fuel cell/supercapacitor hybrid source based on differential flatness control. IEEE Trans Vehicular Technology 2010; 59(6):2700-10.

[34] Cardenas A, Agbossou K, Henao N. Development of power interface with FPGA-based adaptive control for PEMFC system. IEEE Trans Energy Conversion 2015; 30(1):296-306.

[35] Kabalo M, Paire D, Blunier B, Bouquain D, Simoes MG, Miraoui A. Experimental validation of high-voltage-ratio low-input-current-ripple converters for hybrid fuel cell supercapacitor systems. IEEE Trans Vehicular Technology 2012; 61(8):3430-40.

[36] Lee JY, Jeong YS, Han BM. A two-stage isolated/bidirectional DC/DC converter with current ripple reduction technique. IEEE Trans Ind Electron 2012; 59(1):644-6.

[57] Wang P, Zhou L, Zhang Y, Li J, Sumner M. Input-parallel output-series DC/DC boost converter with a wide input voltage range for fuel cell vehicles. IEEE Trans Vehicular Technology 2017; 66(9): 7771-81.

[38] Kim JS, Choe GY, Kang HS, Lee BK. Robust low frequency current ripple elimination algorithm for grid-connected fuel cell systems with power balancing technique. Renewable Energy 2011; 36(5):1392-400.

[39] Shireen W, Nene BR. Input ripple current compensation using DSP control in reliable fuel cell power systems. Int J Hydrogen Energy 2012; 37(9):7807-13.

[40] Somaiah B, Agarwal V, Choudhury SR, Duttagupta SP, Govindan K. Analysis and comparative study of pulsating current of fuel cells by inverter load with different power converter topologies. Int J Hydrogen Energy 2011; 36(22):15018-28.

[41] Cao L, Loo KH, Lai YM. Output-impedance shaping of bidirectional DAB DC–DC converter using double-proportional-integral feedback for near-ripple-free DC bus voltage regulation in renewable energy systems. IEEE Trans Power Electron 2016; 31(3):2187-99.

[42] Cao L, Loo KH, Lai YM. Systematic derivation of a family of output-impedance shaping methods for power converters—a case study using fuel cell-battery-powered single-phase inverter system. IEEE Trans Power Electron 2015; 30(10):5854-69.

[43] Cao L, Loo KH, Lai YM. Frequency-adaptive filtering of low-frequency harmonic current in fuel cell power conditioning systems. IEEE Trans Power Electron 2015; 30(4):1966-78.

[44] Maciel RS, Freitas LC, Coelho EAA, Vieira JB, Freitas LCG. Front-end converter with integrated PFC and DC/DC functions for a fuel cell UPS with DSP-based control. IEEE Trans Power Electron 2015; 30(8):4175-88.

[45] Ahmad AA, Abrishamifar A, Samadi S. Low-frequency current ripple reduction in front-end boost converter with single-phase inverter load. IET Power Electron 2012; 5(9):1676-83.

[46] Li WH, Fan LL, Zhao Y, He XN, Xu DW, Wu B. High-step-up and high-efficiency fuel-cell power-generation system with active-clamp flyback-forward converter. IEEE Trans Ind Electron 2012; 59(1):599-610.

[47] Palma L. An active power filter for low frequency ripple current reduction in fuel cell applications. 2010 International Symposium on Power Electronics Electrical Drives Automation and Motion. Pisa, Italy, 14-16 Jun. 2010, p. 1308-13.

[48] Tao H, Duarte JL, Hendrix MA. Line-interactive UPS using a fuel cell as the primary source. IEEE Trans Ind Electron 2008; 55(8):3012-21.

1   [49] Kan JR, Xie SJ, Wu YY, Tang Y, Yao ZL, Chen R. Single-stage and boost-voltage

2   grid-connected inverter for fuel-cell generation system. IEEE Trans Ind Electron 2015;

3   62(9):5480-90.

4   [50] Liu XH, Li H, Wang Z. A fuel cell power conditioning system with

5   low-frequency ripple-free input current using a control-oriented power pulsation

6   decoupling strategy. IEEE Trans Power Electron 2014; 29(1):159-69.

7   [51] Mazumder SK, Burra RK, Acharya K. A ripple-mitigating and energy-efficient fuel

8   cell power-conditioning system. IEEE Trans Power Electron 2007; 22(4):1437-52.

9   [52] Leu CS, Li MH. A novel current-fed boost converter with ripple reduction for

10 high-voltage conversion applications. IEEE Trans Ind Electron 2010; 57(6):2018-23.

11 [53] Kwon JM, Kim EH, Kwon BH, Nam KH. High-efficiency fuel cell power

12 conditioning system with input current ripple reduction. IEEE Trans Ind Electron 2009;

13 56(3):826-34.

14 [54] Wang Y, Choi SY, Lee EC. Efficient and ripple-mitigating DC/DC converter for

15 residential fuel cell system. Int J Electrical Power & Energy Systems 2009; 31(1):43-9.

16 [55] Wu JC, Wu KD, Jou HL, Wu ZH, Chang SK. Novel power electronic interface for

17 grid-connected fuel cell power generation system. Energy Conversion and Management

18 2013; 71(1):227-34.

19 [56] Mustafa AA, Esam HI. A high voltage ratio and low stress DC/DC converter with

20 reduced input current ripple for fuel cell. Renewable Energy 2015; 82: 35-43.

[57] Itoh JI, Hayashi F. Ripple current reduction of a fuel cell for a single-phase isolated converter using a DC active filter with a center tap. IEEE Trans Power Electron 2010; 25(3):550-6.

[58] Abeywardana DBW, Hredzak B, Agelidis VG. An input current feedback method to mitigate the DC-side low-frequency ripple current in a single-phase boost inverter. IEEE Trans Power Electron 2016; 31(6):4594-603.

[59] Abeywardana DBW, Hredzak B, Agelidis VG. A rule-based controller to mitigate DC-side second-order harmonic current in a single-phase boost inverter. IEEE Trans Power Electron 2016; 31(2):1665-79.

[60] Zhu GR, Tang SC, Chen CY, Tse CK. Mitigation of low-frequency current ripple in fuel-cell inverter systems through waveform control. IEEE Trans Power Electron 2013; 28(2):779-92.

[61] Zhu GR, Wang HR, Liang B, Tan SC, Jiang J. Enhanced single-phase full-bridge inverter with minimal low-frequency current ripple. IEEE Trans Ind Electron 2016; 63(2):937-43.

[62] Galvez JM, Ordonez M. Swinging bus operation of inverters for fuel cell applications with small DC-link capacitance. IEEE Trans Power Electron 2015; 30(2):1064-75.

[63] Galvez JM, Ordonez M. Swinging bus technique for ripple current elimination in fuel cell power conversion. IEEE Trans Power Electron 2014; 29(1):170-8.

[64] Liu XH, Li H. An electrolytic-capacitor-free single-phase high-power fuel cell converter with direct double-frequency ripple current control. IEEE Trans Ind Applications 2015; 51(1):297-308.

[65] Wai RJ, Lin CY. Active low-frequency ripple control for clean-energy power-conditioning mechanism. IEEE Trans Ind Electron 2010; 57(11):3780-92.

[66] Bizon N. A new topology of fuel cell hybrid power source for efficient operation and high reliability. J Power Sources 2011; 196(6):3260-70.

[67] Cheng SJ, Lo YK, Chiu HJ, Kuo SW. High-efficiency digital-controlled interleaved power converter for high-power PEM fuel-cell applications. IEEE Trans Ind Electron 2013; 60(2):773-80.

[68] Giustiniani A, Petrone G, Spagnuolo G, Vitelli M. Low-frequency current oscillations and maximum power point tracking in grid-connected fuel-cell-based systems. IEEE Trans Ind Electron 2010; 57(6):2042-53.

[69] Shireen W, Nene HR. Input ripple current compensation using DSP control in reliable fuel cell power systems. Int J Hydrogen Energy 2012; 37(9):7807-13.

[70] Shireen W, Rahul A, Kulkarni M. Analysis and minimization of input ripple current in PWM inverters for designing reliable fuel cell power systems. J Power Sources 2006; 156(2):448-54.

[71] Ramos-Paja CA, Arango E, Giral R, Saavedra-Montes AJ, Carrejo C. DC/DC pre-regulator for input current ripple reduction and efficiency improvement. Electric Power Systems Research 2011; 81(11):2048-55.

[72] Zhang L, Ruan XB, Ren XY. Second-harmonic current reduction and dynamic performance improvement in the two-stage inverters: an output impedance perspective. IEEE Trans Ind Electron 2015, 62(1): 394-404.

[73] Ostroznik S, Bajec P, Zajec P. A study of a hybrid filter. IEEE Trans Ind Electron 2010; 57(3):935-42.

[74] Zhan YD, Guo YG, Zhu JG, Li L. Performance comparison of input current ripple reduction methods in UPS applications with hybrid PEM fuel cell/supercapacitor power sources. Int J Electrical Power and Energy Systems 2015; 64(1):96-103.

[75] Zhan YD, Guo YG, Zhu JG, Wang H. Intelligent uninterruptible power supply system with backup fuel cell/battery hybrid power sources. J Power Sources 2008; 179(2): 745-53.